Particle Sizing in Dense Suspensions With Multiwavelength Photon Migration Measurements

Sarabjyot Singh Dali, John C. Rasmussen, Yingqing Huang, Ranadhir Roy, and Eva M. Sevick-Muraca
The Photon Migration Laboratories, Dept. of Chemistry, Texas A&M University, College Station, TX 77842

DOI 10.1002/aic.10370
Published online February 23, 2005 in Wiley InterScience (www.interscience.wiley.com).

Characterization of dense polydisperse suspensions, with mean diameters 143 and 226 nm and volume fractions ranging from 0.03 to 0.27, was conducted using time-dependent measurements of multiply scattered light. Frequency-domain photon migration measurements of isotropic scattering coefficients at wavelengths between 488 and 828 nm were found to agree with those predicted from the Mie theory and the polydisperse hard-sphere Percus–Yevick model. The wavelength-dependent isotropic scattering data were then used to successfully recover the particle size distribution and volume fraction of the suspensions, by minimizing a nonlinear least-squares problem. The mean particle size and volume fractions were recovered within an error range of 0–15.53 and 0–24%, respectively, compared with dynamic light scattering results and experimentally measured volume fractions. © 2005 American Institute of Chemical Engineers *AIChE J,* 51: 1116–1124, 2005

Keywords: frequency-domain photon migration, concentrated suspensions, polydisperse static structure factor, hard-sphere Percus–Yevick approximation, particle sizing, multiple scattering, nonlinear least-squares minimization, genetic algorithms

Introduction

Characterization of dense colloidal suspensions by optical or acoustical ensemble scattering techniques may offer the opportunity for nondestructive and noninvasive process control and product quality measurement.[1] Yet the inverse problem associated with determining particle size distribution [$f(x)$] and volume fraction (ϕ) is made difficult by the influence of nonrandom particle orientation, governed predominantly by volume-exclusion effects as well as other forces, such as electrostatic, depletion, and van der Waals forces.[2] The structure of dense suspensions exerts an impact on both the static and dynamic scattered fields, requiring one to account for ordering effects when solving the inverse problems for characterization of dense colloidal suspensions. Table 1 summarizes the static and dynamic optical ensemble techniques, their measurements, and the integral equations that represent their respective inverse problems for characterizing dilute and dense suspensions. Because acoustic ensemble approaches are being increasingly implemented for particle characterization in industry, they are also included in Table 1.

Of the static light-scattering measurements, turbidity and angular light scattering (ALS, also termed diffraction) measurements are restricted to dilute suspensions that do not multiply scatter light. Because the measurements consist of monitoring the amount of light scattered out of an optical path (L), dense suspensions that multiply scatter light back into the path represent invalid turbidity and ALS samples. Although one can alleviate multiple scattering by decreasing the path length and/or index matching, wavelength-dependent turbidity or ALS measurements are typically not conducted for particle characterization in dense suspensions. Dynamic light scattering (DLS) is similar to turbidity, in that it does not account for multiply scattered light, but instead reflects the collective Brownian motion of the particles that contribute to the decay of the autocorrelation function. From the ensemble measurement

Correspondence concerning this article should be addressed to E. M. Sevick-Muraca at eva-m-sevick@tamu.edu.

Table 1. Ensemble Methods for Particle Sizing*

Measurement Method	Measured Quantity	A priori Information	Fredholm's Equation	References
Turbidity (Static) (Dilute)	Intensity $I(\lambda)$ at $\theta = 0°$	$n\&m$	$-\frac{1}{L}\ln\left[\frac{I(\lambda)}{I_o(\lambda)}\right] = \mu_s(\lambda) = \int_0^{\infty}\frac{3Q_{scat}(x,n,\lambda)}{2x}\phi f(x)dx$	Garcia-Rubio et al.[21]
ALS (Static) (Dilute)	Intensity $I(\lambda)$ at several θ	$n\&m$	$\ln\left[\frac{I(\lambda)}{I_0(\lambda)}\right]\alpha q_{scat}(x,n,\lambda,\theta) = \int_{V_j}\int_{\Delta\theta_j}\int_{x_i}^{x_j} Nf(x)\frac{dq_{scat}(x,n,\lambda,\theta)}{d\theta}dxd\theta dV$	Frock[22,23]
DLS (Dynamic) (Dilute)	Intensity fluctuations $I(t)$, to obtain $g^2(\tau)$	Solvent viscosity	$g^{(2)}(\tau) = 1 + \beta\lvert g^{(1)}(\tau)\rvert^2$ $g^{(1)}(\tau) = \int_{x_{\min}}^{x_{\max}} f(x)\exp(-Q^2D\tau)dx$ (For concentrated) $D(Q) = D_0\frac{H(Q)}{S(Q)}$	Berne and Pecora[24]
DWS (Dynamic) (Concentrated)	Intensity fluctuations $I(t)$, to obtain $g^2(\tau)$	Cell geometry, $P(s)$, $n\&m$ (point or planar source)	$g^{(2)}(\tau) = 1 + \beta\lvert g^{(1)}(\tau)\rvert^2$ $g^{(1)}(\tau) \propto \int_0^{\infty} \mathrm{P(s)}\exp\left\{-2k_0^2D_0t\frac{[H(q)]}{[S(q)]}\frac{s}{l^*}\right\}ds$	Horne and Davidson[25] Scheffold[8,26]
DTS (Static) (Concentrated)	Transmitted intensity, $I(\lambda)$	$n\&m$	$(1-g)\mu_s(\lambda) = \frac{3}{2}\phi\int_{x_{\min}}^{x_{\max}}\frac{Q_{scat}(x,n,\lambda)[1-g(x,n,\lambda)]}{x}f(x)S(q)dx$	Kaplan et al.[7]
FDPM (Static) (Concentrated)	AC, DC, and PS of the photon density wave	$n\&m$	$\mu_s'(\lambda) = \int_0^{\pi}\frac{12\phi}{k^2}\int_0^{\infty}\frac{f(x_i)}{x_i^3}\int_0^{\infty}\frac{f(x_j)}{x_j^3}F_{i,j}(n,x_i,x_j,\lambda,\theta) \times S_{i,j}(n,x_i,x_j,\lambda,\theta)\sin\theta(1-\cos\theta)dx_idx_jd\theta$	Sun et al.[11]
AS (Static) (Concentrated)	Attenuation coefficient, α, and ultrasonic velocity	Viscosity, specific heat Capacity, thermal expansivity, and conductivity	$\alpha(\omega) = \int_0^{\infty}\alpha(\omega,x)f(x)dx$	McClements[27] Alba et al.[28] Alexander et al.[29]

*$n\&m$ = refractive index of particle and solvent; $H(q)$, hydrodynamic factor; $S(q)$ static structure factor.

of particle diffusion coefficient, characterization of particle size and volume fraction may be obtained from the solution of the inverse problem. Index matching, the use of fiber optics,[3,4] and the use of conventional optical methods to eliminate the predominant multiply scattered signal[5,6] may enable DLS characterization of dense suspensions. Yet again DLS measurements are generally used for dilute suspensions. Efforts to eliminate the predominant multiply scattered light for measurement of the small component of singly scattered light are done at the expense of signal-to-noise ratio (SNR) for both DLS and ALS measurements.

In contrast, diffuse transmission and diffuse wave spectroscopies (DTS and DWS, respectively) entail respective static and dynamic measurements of multiply scattered light and therefore are predisposed to dense colloidal suspensions. DTS measurement consists of determining the isotropic scattering coefficient as a function of wavelength and then inverting for suspension characterization.[7] DWS[8] measures the fluctuation of multiply scattered light arising from the collective Brownian motion of the particles in colloids. It depends on a priori information of the optical properties for prediction of the distribution of path lengths traveled by photons to determine the ensemble particle diffusion coefficient, and from the inverse solution, size information.

Wavelength-dependent, time-resolved diffuse transmission and reflectance measurements are the subject of this contribution and can be accomplished in either the time domain or the frequency domain.[9-11] In simple terms, time-dependent techniques measure the distribution of photon times-of-flight to determine the absorption and isotropic scattering coefficients of multiply scattering, dense suspensions with accuracy and precision.[12] Although time-resolved diffuse measurements have temporal resolution of photon transport on the order of pico- to nanoseconds, dynamic measurements assess particle motion on the order of microseconds to milliseconds. Few dynamic time-resolved measurements have been attempted[13] and, to date, there have been no static measurements of wavelength-dependent isotropic scattering for characterization of dense colloidal suspensions. Prior work in our research group has focused on conducting measurements of isotropic scattering at one wavelength as a function of known volume fraction to extract size and interaction parameters. However, volume fraction and concentration are often unknown. In this contribution we demonstrate the added use of multiwavelength measurements of isotropic scattering to determine size information as well as the volume fraction of dense colloidal suspensions.

In the following we extend frequency-domain photon migration (FDPM) for multiwavelength measurements of isotropic scattering to demonstrate recovery of particle size and volume fraction using a polydisperse hard-sphere exclusion model and global and local search routines for nonlinear optimization. Below, the FDPM approach is first briefly outlined, followed by an experimental section that describes the samples, multiwavelength FDPM measurements, and optimization algorithms used.

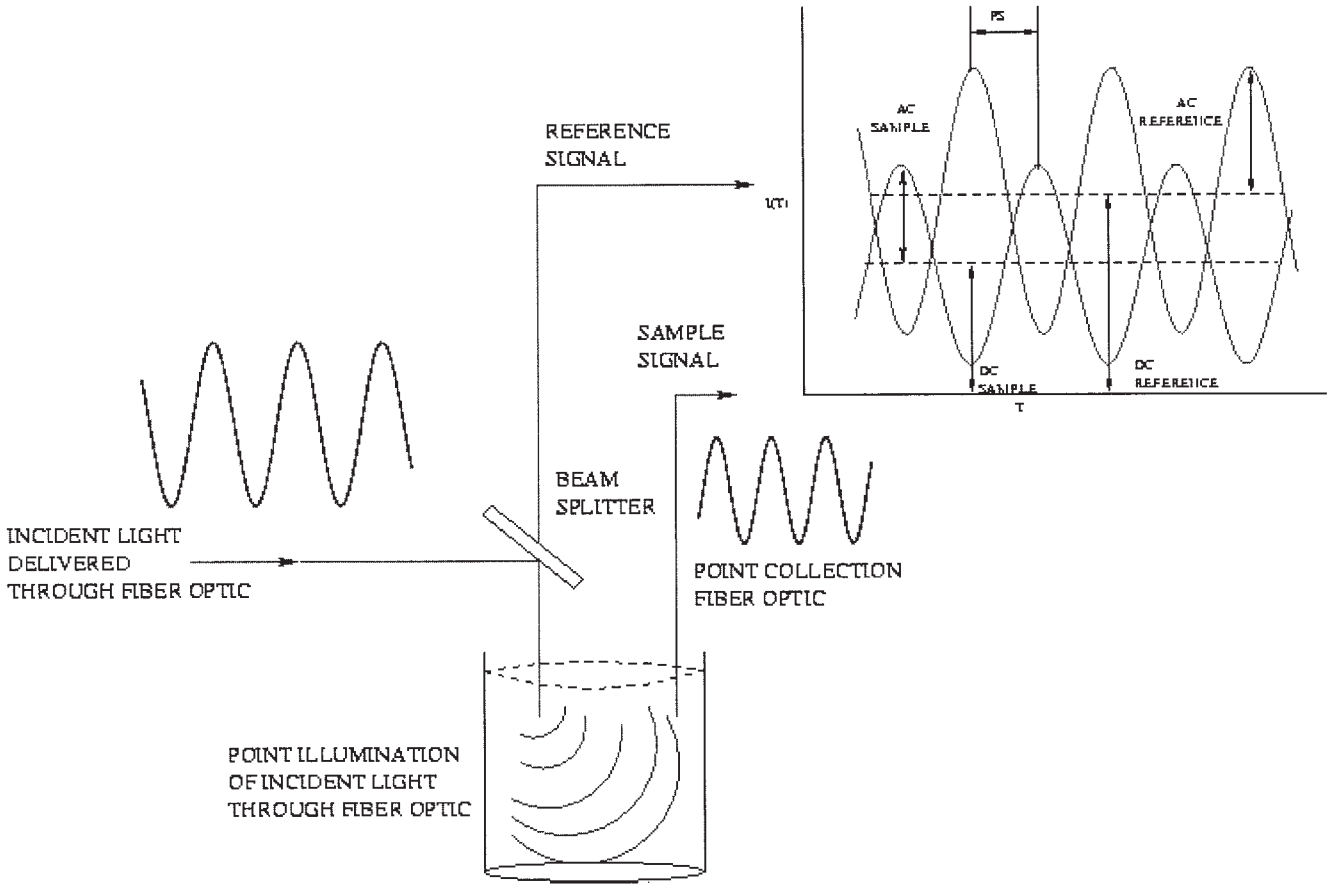

Figure 1. Principle of frequency-domain photon migration and data acquisition.

Theory and Background

FDPM theory

Figure 1 embodies the principles of FDPM measurement as conducted in this work. Intensity-modulated light (typically modulated from 30 to 100's of MHz) is launched into a multiply scattering medium via a fiber optic. As the light propagates through the medium, it is phase shifted and amplitude attenuated with respect to the incident wave, arising from the optical properties of the medium. The phase and amplitude of the propagated wave are determined at known distances away from the point of incident illumination. The propagation of the photon density wave can be modeled using the diffusion approximation to the radiative transfer equation, which is valid when the photon trajectory becomes completely randomized. The governing equation in the frequency domain is expressed as

$$\nabla \cdot [D\nabla\Phi(\bar{r}, \omega)] - \left(\mu_a + \frac{i\omega}{c}\right)\Phi(\bar{r}, \omega) + S(\bar{r}, \omega) = 0 \qquad (1)$$

where $\Phi(\bar{r}, \omega)$ is the complex fluence describing the characteristics of the photon density wave at position $\bar{r}$ and modulated at angular frequency ω; $S(\bar{r}, \omega)$ is the isotropic source term; c is the speed of light in the medium; and D is the optical diffusion coefficient, which is defined as

$$D = \frac{1}{3(\mu_s' + \mu_a)} \qquad (2)$$

Here μ_a is the absorption coefficient; $\mu_s' = (1 - g)\mu_s$ is the isotropic scattering coefficient; and g, the anisotropy parameter, is the mean cosine of the scattering angle.

Herein, the analytical solution to Eq. 1 for the case of a sinusoidally intensity-modulated point of illumination in an infinite medium is used to predict $\Phi(r, \omega) = I_{AC}\exp(-i\mathrm{PS})$, where I_{AC} is the amplitude of the photon density wave; PS is the phase lag that occurs between the incident and detected wave that has propagated within the medium. The time average photon density at the detector is the DC component of the waveform.

From FDPM measurements of AC, DC, and PS as a function of distance away from the point of illumination, the optical properties of isotropic scattering and absorption coefficient can be accurately fit to the solution of Eq. 1 (see Sun et al.[14] for details).

Forward problem

The elastic wavelength-dependent isotropic scattering coefficient, of a concentrated colloidal suspension, is dependent on individual particle scattering efficiencies as well as their cor-

Table 2. Characterization Results of Polydisperse Suspensions Using Dynamic Light Scattering

Dispersion	Mean (nm)	Spread (nm)	Polydispersity (%)
Dow 755	223.6 ± 3.6	32.4 ± 15.2	14.5
Dow 788	143.6 ± 3.7	35.0 ± 7.2	24.4

related position, as indicated by the following integral equation:

$$\mu_s' = \int_0^{\pi} \frac{12\phi}{k^2} \int_0^{\infty} \frac{f(x_i)}{x_i^3} \int_0^{\infty} \frac{f(x_j)}{x_j^3} \times F_{i,j}(n, x_i, x_j, \lambda, \theta) S_{i,j}(q, x_i, x_j, \phi) \sin\theta(1 - \cos\theta) dx_j dx_i d\theta \quad (3)$$

where $F_{i,j}$ is the binary form factor evaluated by Mie scattering, expressed as[15]

$$F_{ij}(q, x_i, x_j) = \mathrm{Re}(f_{1,i} f_{1,j}^* + f_{2,i} f_{2,j}^*) \quad (4)$$

where $f_{1,i}$ and $f_{2,i}$ are the scattering amplitudes in two orthogonal polarization states arising from a particle with size x_i; and the terms $f_{1,j}^*$ and $f_{2,j}^*$ are the complex conjugates of $f_{1,j}$ and $f_{2,j}$, respectively. The term q is the scattering vector and is given as $2k \sin(\theta/2)$, where k is the wavenumber of the medium ($2\pi m/\lambda$); m is the refractive index of the surrounding medium; λ is the wavelength of the incident radiation; θ is the scattering angle; ρ is the total number density of the particles; x_i and x_j are the particle diameters i and j, respectively; and $f(x_i)$ and $f(x_j)$ are the volume-based particle size distributions, which are assumed to have a known form for the inverse problem. The term $S_{ij}(q, x_i, x_j, \phi)$ is the polydisperse partial static structure factor[16] that accounts for hard-sphere particle interactions within the concentrated suspension of volume fraction ϕ.

Inverse problem

The inverse problem consists of minimizing either a nonlinear absolute or a relative least-squares difference between experimentally measured isotropic scattering functions and those predicted by Eq. 3, to retrieve the particle size distribution parameters and the volume fraction ϕ of the suspension. In this work, we assume particle size distributions to be Gaussian with $\bar{X}$ as the mean particle diameter and σ as the spread of the distribution. Alternatively, we also assume a particle distribution of a more general form as predicted by the Johnson's SB function.[17]

Experimental

Materials used

Samples were prepared from two polystyrene solutions of 143 and 223 nm particle size, from Dow Chemical Company. The solutions were dialyzed to remove residual surfactants and salts arising from the manufacturing process and then characterized using dynamic light scattering (DLS, Zetasizer 3000, Malvern Instruments, Malvern, UK) to obtain the mean particle size, spread of the distribution, and the polydispersity. Table 2 lists the results. The solids volume fractions of the dialyzed suspensions were determined by evaporation measurements conducted at 80°C. From each dialyzed suspension of the two particle sizes, 100-mL volumes at particle volume fractions of 0.03, 0.10, 0.18, and 0.27 were prepared by dilution with deionized water and sodium chloride to achieve ionic strengths of 120 mM of NaCl.

FDPM instrumentation

FDPM measurements were made on all the samples at seven different wavelengths (488, 514, 568, 650, 687, 785, and 828 nm), using both external modulation of laser light and direct modulation of laser diodes. Although the details of FDPM instrumentation and method have been presented elsewhere,[14,18] a brief description of both approaches is presented here.

Figure 2 is the setup using direct modulation of laser diodes to gather FDPM data at 650 through 828 nm. As shown, a laser diode (650-nm TOLD 9442M, 687-nm HL 6738MG, and 785-nm DL7140-201, all obtained from Thorlabs, Newton, NJ) was modulated with a radio frequency (RF) signal (Signal Generator 2022A; Marconi Instruments, Mountain View, CA) to produce an intensity-modulated light at modulation frequency ω. The beam was split to produce reference and sample beams. The reference beam was sent directly to a photomultiplier tube (PMT, Model H6573, Hamamatsu Corp., Japan) for assessment of incident modulated light. The sample beam was delivered to the polystyrene suspension by an optical fiber (1000 μm FT-1.0-EMT, Thorlabs). Another fiber, located at a distance r from the source fiber, was used to collect the diffused light and deliver it to the sample PMT. Both PMTs were gain modulated with another RF signal at a modulation frequency of $\omega + \Delta\omega$ generated from a slave generator (Signal Generator 2022A, Marconi Instruments), which was phase locked with the master signal generator by a 10-MHz signal. The signals at the reference and sample PMTs were mixed with the RF from the slave generator to give output signals at frequency $\Delta\omega$. The signals were amplified by transimpedance amplifiers and then acquired using an internally authored Labview program, which retrieves the phase differences between the reference and sample beams, as well as their amplitudes.

To collect data at lower wavelengths (488, 514, and 568 nm), light from an argon–krypton laser (Model 643R-AP-A01, Melles Griot®, Barloworld Scientific, Carlsbad, CA) was modulated externally with an electro-optic modulator (Model 350-160, Conoptics, Danbury, CT), as shown in Figure 3. An additional amplifier (Model 3100LA, Electronics & Innovation, Rochester, NY) was also required to amplify the RF signal from the signal generator to the modulator. For both instruments described above, data were collected as the distance between collected and incident light r, varied from 3 to 15 mm at modulation frequencies ranging from 70 to 90 MHz. From values of DC and PS, values of μ_s' and μ_a were obtained.

Optimization procedure

The particle size distributions and volume fraction of the dense colloidal suspensions were determined by minimizing

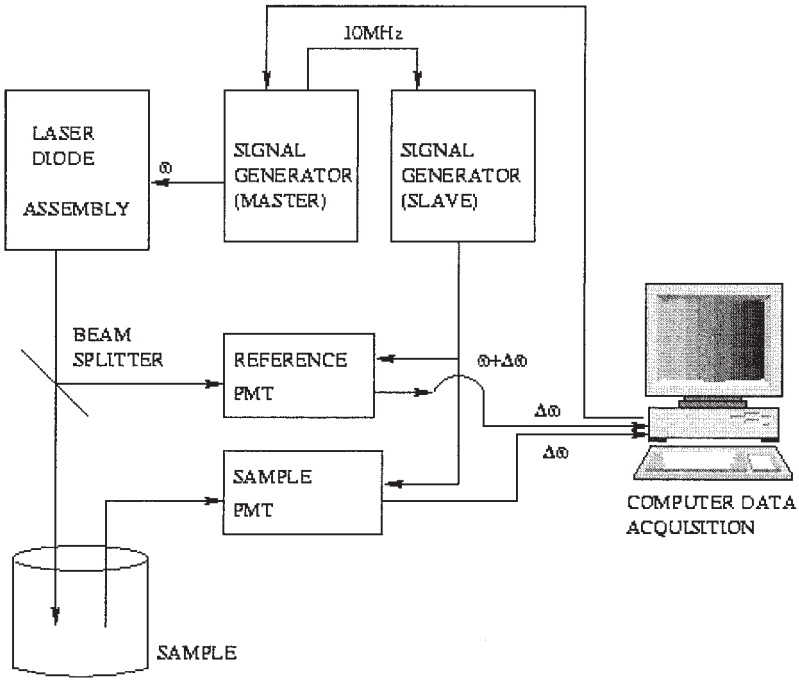

Figure 2. Laser diode setup for frequency-domain photon migration.

the absolute and relative squared differences between experimentally measured isotropic scattering coefficients, $\mu_s'^e(\lambda)$ at each wavelength and $\mu_s'^c(\lambda)$, or that predicted by Eq. 3. The three objective functions

$$\chi_1^2 = \sum_{\lambda_i} (\mu_s'^c - \mu_s'^e)^2 \qquad \chi_2^2 = \sum_{\lambda_i} \left(\frac{\mu_s'^c - \mu_s'^e}{\mu_s'^e} \right)^2$$

$$\chi_3^2 = \sum_{\lambda_i} \left(\frac{\mu_s'^c - \mu_s'^e}{\mu_s'^c} \right)^2$$

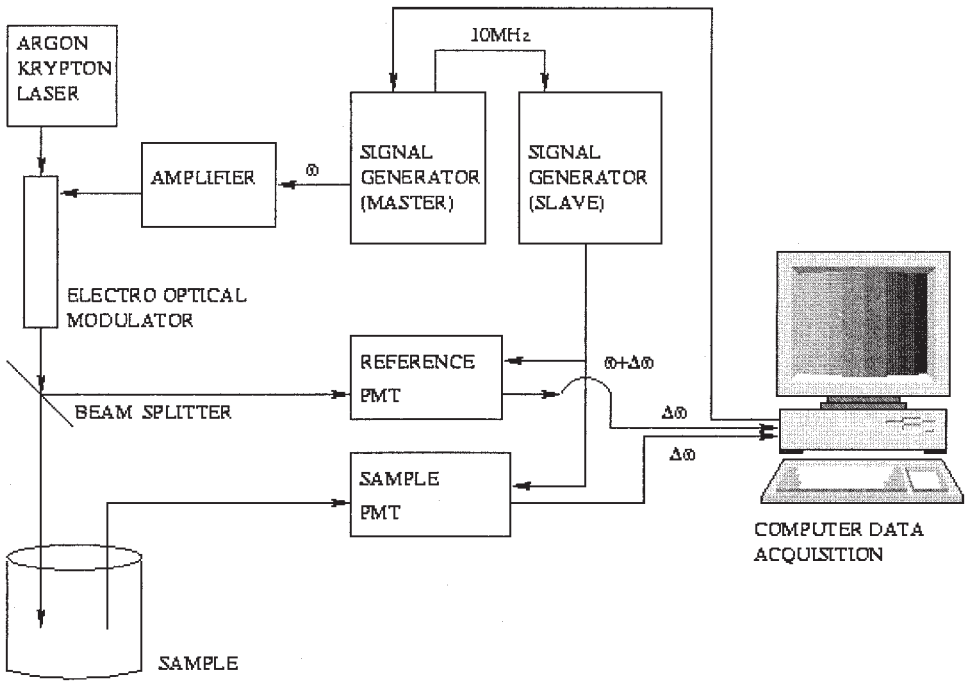

Figure 3. Argon–krypton gas laser setup for frequency-domain photon migration.

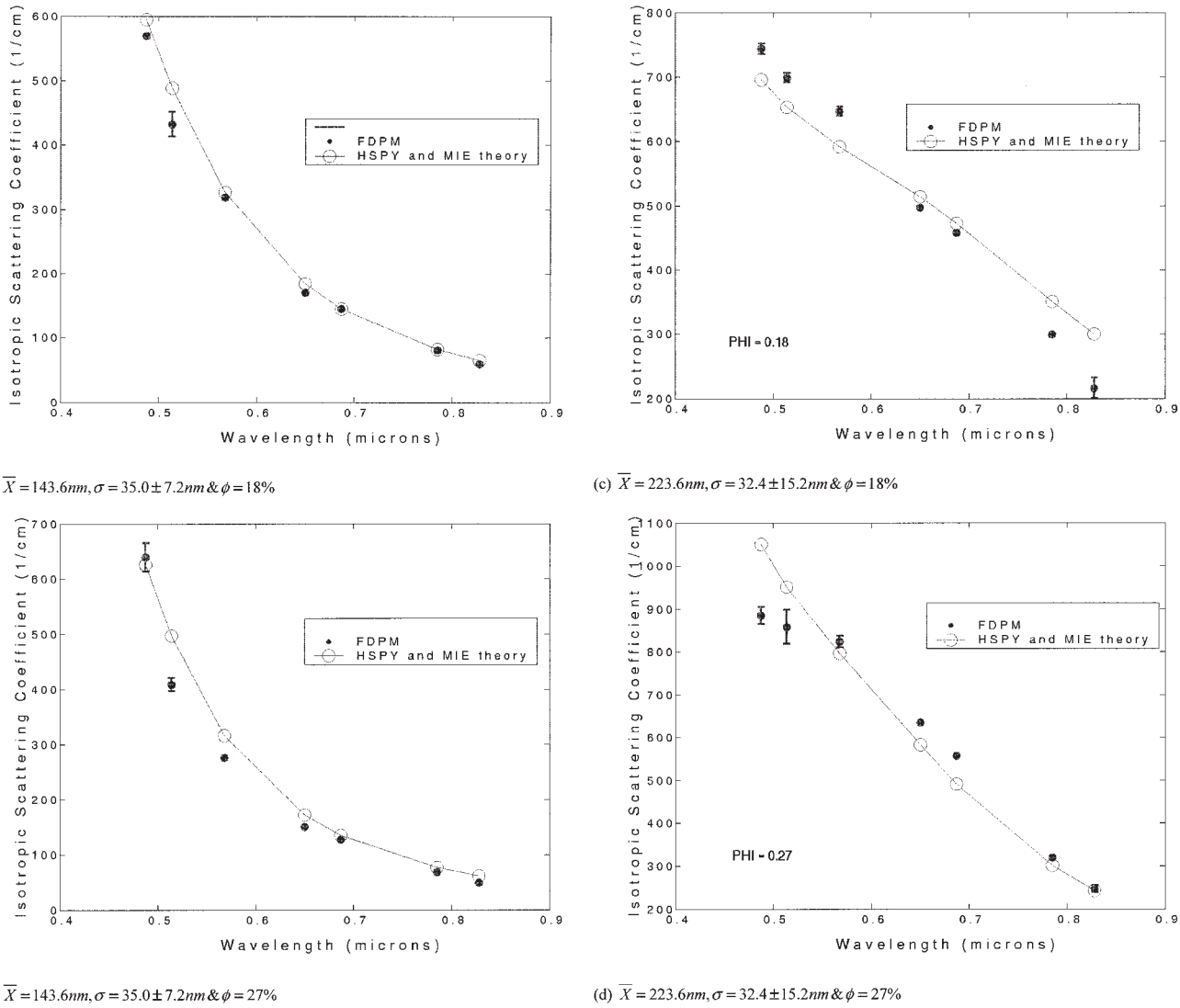

(a) $\overline{X} = 143.6nm, \sigma = 35.0 \pm 7.2nm \& \phi = 18\%$

(c) $\overline{X} = 223.6nm, \sigma = 32.4 \pm 15.2nm \& \phi = 18\%$

(b) $\overline{X} = 143.6nm, \sigma = 35.0 \pm 7.2nm \& \phi = 27\%$

(d) $\overline{X} = 223.6nm, \sigma = 32.4 \pm 15.2nm \& \phi = 27\%$

Figure 4. FDPM (solid points) and model prediction (open symbols connected by line) for an assumed Gaussian distribution.

Error bars represent the standard error propagated from the measurements. Model prediction used Mie theory with hard-sphere Percus–Yevick approximation to predict structure.

were minimized using genetic algorithms and Matlab® (The MathWorks, Natick, MA) local search subroutines. Because genetic algorithms render values close to the global optimum, they were used to obtain initial guesses for local search Matlab algorithms. The genetic algorithm software coded by Houck and colleagues[19,20] was used and implemented in Matlab. The local search algorithms used were *Fmincon* and *Lsqnonlin*. *Fmincon* uses sequential quadratic programming (SQP), and solves a quadratic programming (QP) subproblem at each iteration. *Lsqnonlin* uses a subspace trust region method based on the interior-reflective trust region method with bounds placed on the estimates. Bounds considered for the Gaussian distribution are $\bar{X}$ (50–1000 nm), σ (5–50 nm), and ϕ (1–40%). The local search convergence criteria required a level of no greater than 10^{-12} absolute change in the estimates on the scattering prediction before the final iteration.

The inverse problem was solved for two cases in which (1) ϕ was assumed known and the distribution parameters ($\bar{X}$, σ) were estimated, and (2) all three parameters—$\bar{X}$, σ, and ϕ—were considered unknown.

Results and Discussion

The interactions between the charged particles have been modeled as effective hard spheres. This is true for the suspending fluid containing 120 mM sodium chloride, which screened repulsive electrostatic forces. As can be observed from Figure 4, the hard-sphere Percus–Yevick (HSPY) structure factor model for a polydisperse system of particles accounts for particle interactions and is well able to describe the experimental data, thus validating the use of the HSPY model for concentrated suspensions.

Tables 3 and 4 list the final results for minimization assuming a Gaussian distribution, using relative least squares (χ_2^2 and

Table 3. Minimization Results for Dow 788 for Assumed Gaussian Distribution*

Function Minimized	Volume Fraction	Local Algorithm: Three Unknowns and Residual			
		$\bar{X}$	σ	ϕ	Residual
$\chi_2^2 = \sum_{\lambda_i} \left(\frac{\mu_s'^c - \mu_s'^e}{\mu_s'^e} \right)^2$	0.03	121.30	5.50	0.043	0.007681
	0.10	144.42	6.04	0.096	0.003749
	0.18	142.96	7.87	0.191	0.012318
	0.27	156.16	6.26	0.314	0.031741
$\chi_2^2 = \sum_{\lambda_i} \left(\frac{\mu_s'^c - \mu_s'^e}{\mu_s'^c} \right)^2$	0.03	121.03	9.61	0.042	0.007752
	0.10	140.20	11.51	0.096	0.003740
	0.18	143.65	10.10	0.178	0.011790
	0.27	148.20	13.93	0.346	0.031545

*$\bar{X}$ = 143.6 nm; σ = 35.0 ± 7.2 nm.

χ_3^2). Least-squares functions of χ_1^2 did not perform well because errors are squared and outliers overly influenced the results. The minimization procedure is significantly affected by the initial guess value of the mean particle size. Consequently, we found that the genetic algorithms provided an efficient means of providing the first initial guess value for all subsequent local searches.

The parameters of the distribution $f(x)$ obtained from relative least-squares functions predict the mean values closely compared to those obtained from DLS measurements of diluted suspensions. As shown in Figure 5 the relative error for recovery of mean particle size $\bar{X}$ was between 0 and 15.53% for $\bar{X}$ = 143.6 nm and 1.83 and 11.90% for $\bar{X}$ = 223.6 nm. The results for a more general SB distribution (which can take into account any skewness in the form of the particle size distribution) show the same trend for inversion of the data. In addition, the mean particle size predictions are more accurate for the higher volume fraction samples ($\phi > 0.03$).

Volume fraction predictions are found to be in good agreement with experimental volume fractions. The relative error for recovery of particle volume fraction was between 0.96 and 24% for $\bar{X}$ = 143.6 nm and 0 and 9.03% for $\bar{X}$ = 223.6 nm. When the volume fraction was assumed known, the inversion of data recovered the mean particle sizes that were accurate (data not shown for brevity). These observations validate the use of the structure factor model for concentrated suspensions. It is notable that the mean of the particle size can be determined along with the volume fractions when multiwavelength measurements are made. Single-wavelength measurements do not yield enough information for determination of size without a priori information of concentration.[11]

Summary

Particle sizing in a dense colloidal suspension using FDPM with multiple wavelengths is possible by accounting for interaction forces among different sizes of particles. This has been achieved by using a most general model for polydisperse interacting systems and finding a global minimum of the optimization problem by first using genetic algorithms and then using local search algorithms to recover $f(x)$ and ϕ. FDPM has proven to be a powerful tool, providing multiple wavelength data using a discrete set of laser diodes and gas lasers for the inverse problem of particle characterization. Because FDPM has the ability to make independent measurements of the scattering and the absorption coefficients in dense multiply scattering systems, common instruments working at several wavelengths provided by laser diode arrays could be used to determine the particle sizes at industrially relevant concentra-

Table 4. Minimization Results for Dow 755 for Assumed Gaussian Distribution*

Function Minimized	Volume Fraction	Local Algorithm: Three Unknowns and Residual			
		$\bar{X}$	σ	ϕ	Residual
$\chi_2^2 = \sum_{\lambda_i} \left(\frac{\mu_s'^c - \mu_s'^e}{\mu_s'^e} \right)^2$	0.03	197.00	23.70	0.029	0.003827
	0.10	204.00	24.20	0.096	0.007870
	0.18	206.95	20.34	0.176	0.010433
	0.27	219.37	10.58	0.245	0.001981
$\chi_2^2 = \sum_{\lambda_i} \left(\frac{\mu_s'^c - \mu_s'^e}{\mu_s'^c} \right)^2$	0.03	196.88	24.30	0.029	0.003829
	0.10	203.84	25.17	0.096	0.007831
	0.18	206.84	21.89	0.176	0.010353
	0.27	219.50	10.35	0.246	0.002017

*$\bar{X}$ = 223.6 nm; σ = 32.4 ± 15.2 nm.

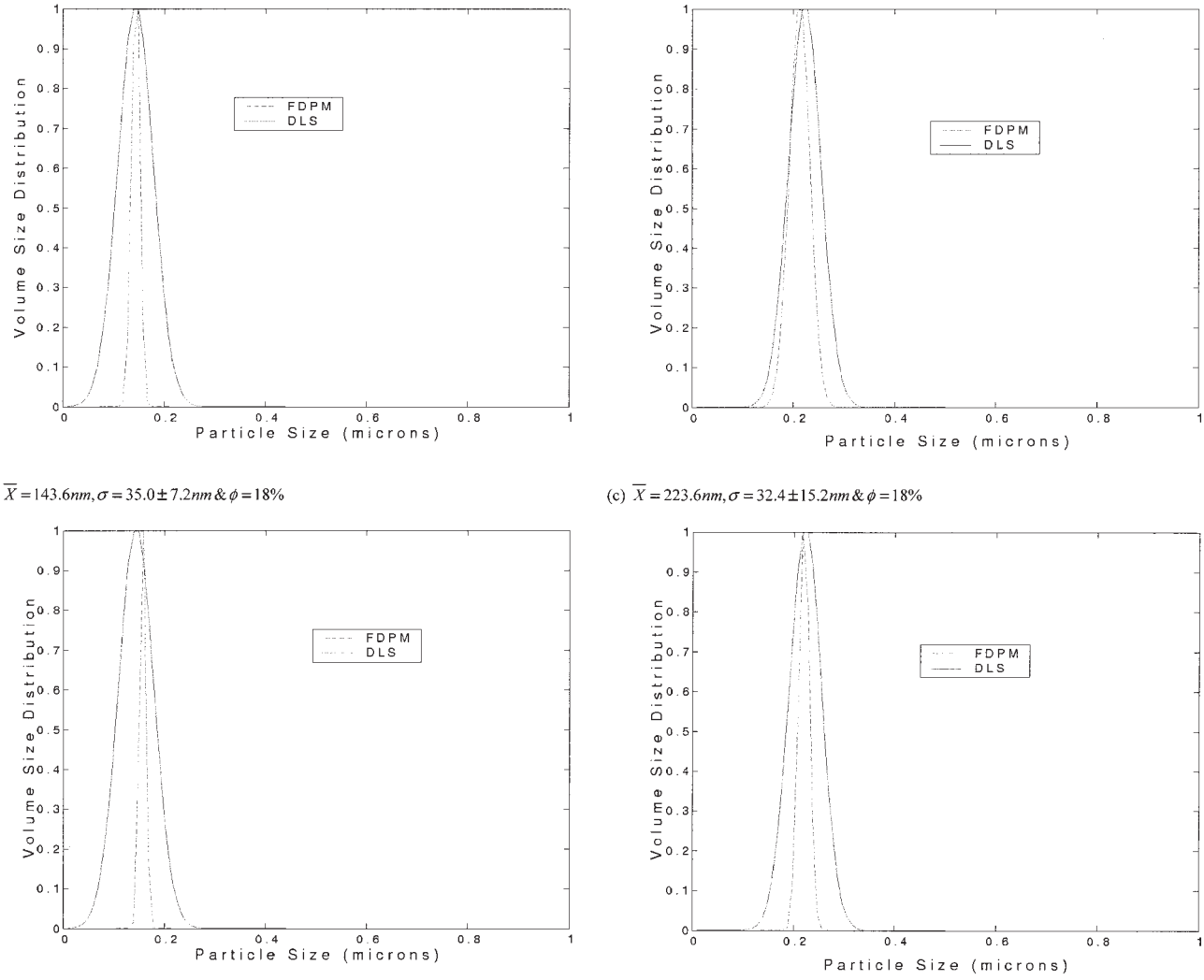

(a) $\overline{X} = 143.6nm, \sigma = 35.0 \pm 7.2nm \& \phi = 18\%$

(c) $\overline{X} = 223.6nm, \sigma = 32.4 \pm 15.2nm \& \phi = 18\%$

(b) $\overline{X} = 143.6nm, \sigma = 35.0 \pm 7.2nm \& \phi = 27\%$

(d) $\overline{X} = 223.6nm, \sigma = 32.4 \pm 15.2nm \& \phi = 27\%$

Figure 5. Comparison between experiment (dashed) and actual particle size distribution (solid) assuming a Gaussian distribution.

tions. Finally, the first principles model of volume exclusion for a hard-sphere suspension enables characterization of dense *spherical* colloidal suspensions. Although multiply scattered light provides a single length scale of an isotropic scattering length to which an effective cross-sectional diameter can be determined, particle interactions may be dramatically influenced by shape. Because there are no analytical solutions for nonspherical, polydisperse particles, the extrapolation of time-dependent measurements for characterizing dense, nonspherical suspensions remains questionable.

Acknowledgments

This work was supported in part by National Science Foundation Grant CTS-0213280.

Notation

c = velocity of light in the medium
D = diffusion coefficient
$f(x)$ = particle size distribution
$f(x_i)$ = volume-based particle size distribution of particle i
$f(x_j)$ = volume-based particle size distribution of particle j
$f_{1,i}, f_{2,i}$ = scattering amplitudes in two orthogonal polarization states
$f^*_{1,j}, f^*_{2,j}$ = complex conjugates of the scattering amplitudes in two orthogonal polarization states
F_{ij} = binary form factor for two particles of different size
g = average of the cosine of the scattering angle
k = wavenumber in vacuum
m = refractive index of the surrounding medium
n = refractive index of the particle suspended in the medium
q = scattering vector
r = distance between the source and detector fibers
S_{ij} = partial static structure factor
$S(\bar{r}, \omega)$ = isotropic source term
t = time
x_i = diameter of particle i
x_j = diameter of particle j
$\overline{X}$ = mean particle size from the Gaussian distribution

Greek letters

θ = scattering angle
λ = wavelength of light in the medium

ϕ = total volume fraction of particles
μ_a = absorption coefficient of the medium
μ_s = scattering coefficient
μ_s' = isotropic scattering coefficient
$\mu_s'^c$ = isotropic scattering coefficient calculated from the forward model
$\mu_s'^e$ = isotropic scattering coefficient obtained from experiment
ρ = total number density of particles
σ = spread of the Gaussian distribution
χ^2 = chi square minimization function
ω = angular modulation frequency
Φ = complex fluence

Abbreviations

AC = alternating current generated at the photomultiplier tube (PMT) of the reference light or the light from the sample
ALS = angular light scattering
AS = acoustic spectroscopy
DC = magnitude of direct current generated at the photomultiplier tube (PMT) of the reference light or the light from the sample
DLS = dynamic light scattering
DTS = diffusing transmission spectroscopy
DWS = diffusing wave spectroscopy
FDPM = frequency-domain photon migration
GA = genetic algorithms
HSPY = hard-sphere Percus–Yevick approximation of the static structure factor model
PMT = photomultiplier tube
PS = phase shift
QP = quadratic programming
SNR = signal-to-noise ratio
SQP = sequential quadratic programming

Literature Cited

1. Allen T. *Particle Size Measurement*. Dordrecht, The Netherlands: Kluwer Academic Publishers; 1997.
2. Russel WB, Saville DA, Schowalter WR. *Colloidal Dispersions*. Cambridge, UK: Cambridge Univ. Press; 1989.
3. Meeren VP, Statsny M, Vanderdeelen J, Baert L. Particle sizing of concentrated emulsions using fibre optic quasi-elastic light scattering. *Colloids Surf A*. 1993;76:125-133.
4. Dhadwal HS, Ansari RR, Meyer WV. A fiber-optic probe for particle sizing in concentrated suspension. *Rev Sci Instrum*. 1991;62:2963-2968.
5. Urban C, Schurtenberger P. Characterization of turbid colloidal suspensions using light scattering techniques combined with cross-correlation methods. *J Colloid Interface Sci*. 1998;207:150-158.
6. Segre PN, Megen WV, Pusey PN, Schatzel K, Peters W. Two-colour dynamic light scattering. *J Modern Opt*. 1995;42:1929-1952.
7. Kaplan PD, Dinsmore AD, Yodh AG, Pine DJ. Diffuse-transmission spectroscopy: A structural probe of opaque colloidal mixtures. *Phys Rev E*. 1994;50:4827-4835.
8. Weitz DA, Pine DJ. *Diffusing-Wave Spectroscopy in Dynamic Light Scattering: The Method and Some Applications*, Monograph 49 on the Physics and the Chemistry of Materials, Brown W, ed. Oxford, UK: Clarendon Press; 1995.
9. Sun Z, Sevick-Muraca EM. Inversion algorithms for particle sizing with photon migration measurement. *AIChE J*. 2001;47:148.
10. Huang Y, Sun Z, Sevick-Muraca EM. Assessment of electrostatic interactions in dense colloidal suspensions with multiply scattered light. *Langmuir*. 2002;18:2048-2053.
11. Sun Z, Tomlin CD, Sevick-Muraca EM. Approach for particle sizing in dense polydisperse colloidal suspension using multiple scattered light. *Langmuir*. 2001;17:6142-6147.
12. Gerkin M, Faris GW. High-precision frequency-domain measurements of the optical properties of turbid media. *Opt Lett*. 1999;24:930-932.
13. Yodh AG, Kaplan PD, Pine DJ. Pulsed diffusing-wave spectroscopy: High resolution through nonlinear optical gating. *Phys Rev B*. 1990; 42:4744-4747.
14. Sun Z, Huang Y, Sevick Muraca EM. Precise analysis of frequency domain photon migration measurement for characterization of concentrated colloidal suspensions. *Rev Sci Instrum*. 2002;73:383-393.
15. Bohren CF, Huffman DR. *Absorption and Scattering of Light by Small Particles*. New York, NY: Wiley; 1983.
16. Stell G, Blum L. Polydisperse systems I: Scattering function for polydisperse fluids of hard or permeable spheres. *J Chem Phys*. 1979; 71:42-46.
17. Yu AB, Standish N. A study of particle size distributions. *Powder Technol*. 1990;62:101-118.
18. Kuwana E, Sevick-Muraca EM. Fluorescence lifetime spectroscopy for pH sensing in multiply scattering media with dyes exhibiting multi-exponential decay kinetics. *Biophys J*. 2002;83:1165-1176.
19. Houck CR, Joines JA, Kay MG. A genetic algorithm for function optimization: A Matlab implementation. ACM transactions on mathematical software. Available at http://ie.ncsu.edu/mirage/GAOToolbox/gaot/; 1995.
20. Michalewicz Z, Logan DT, Swaminathan S. Evolutionary operators for continuous convex parameter spaces. Proc of Third Ann Conf on Evolutionary Programming. River Edge, NJ: World Scientific Publishing; 1994:84-97.
21. Elicabe GE, Garcia-Rubio LH. Latex particle size distribution from turbidimetric measurements. *Adv Chem Ser Polym Character*. 1990; 227:83-104.
22. Frock HN. Particle-size determination using angular light—scattering. *ACS Symp Ser*. 1987;332:146-160.
23. Jones MR, Curry BP, Brewster MQ, Leong KH. Inversion of light-scattering measurements for particle size and optical constants: Theoretical study. *Appl Opt*. 1994;33:4025-4034.
24. Berne BJ, Pecora R. *Dynamic Light Scattering*. New York, NY: Dover Publications; 1976.
25. Horne DS, Davidson CM. Application of diffusing wave spectroscopy to particle sizing in concentrated dispersions. *Colloids Surf A*. 1993; 77:1-8.
26. Scheffold F. Particle sizing with diffusing wave spectroscopy. *J Dispersion Sci Technol*. 2002;23:591-599.
27. McClements DJ. Principles of ultrasonic droplet size determination in emulsions. *Langmuir*. 1996;12:3454-3461.
28. Alba F, Crawley GM, Fatkin J, Higgs DMJ, Kippax PG. Acoustic spectroscopy as a technique for the particle sizing of high concentration colloids, emulsions and suspensions. *Colloids Surf A*. 1999;153: 495-502.
29. Alexander KH, Storti G, Morbidelli M. Particle sizing in colloidal dispersions by ultrasound. Model calibration and sensitivity analysis. *Langmuir*. 1999;15:2338-2345.

Manuscript received Dec. 22, 2003, and revision received Jul. 27, 2004.